SAND2007-0871C

Improved Manufacturability of AlGaAs/GaAs Pnp Heterojunction Bipolar Transistors

J. B. Clevenger[a], G. A. Patrizi[a], T. C. Peterson[a], M. J. Cich[a], A. G. Baca[a], J. Klem[a], T. A. Plut[a], T. R. Fortune[b], M. S. Hightower[c], D. Torres[d], S. D. Hawkins[a], and C. T. Sullivan[a]

[a]Sandia National Laboratories, Albuquerque, NM 87185, USA
[b]The Plus Group, Albuquerque, NM, USA
[c]ASAP, Inc., Albuquerque, NM, USA
[d]L&M Technologies, Albuquerque, NM, USA

Specially designed Pnp heterojunction bipolar transistors (HBT's) in the AlGaAs/GaAs material system can offer improved radiation response over commercially-available silicon bipolar junction transistors (BJT's). To be a viable alternative to the silicon Pnp BJT, improvements to the manufacturability of the HBT were required. Utilization of a Pd/Ge/Au non-spiking ohmic contact to the base and implementation of a PECVD silicon nitride hard mask for wet etch control were the primary developments that led to a more reliable fabrication process. The implementation of the silicon nitride hard mask and the subsequent process improvements increased the average electrical yield from 43% to 90%.

Introduction

Pnp transistors are used as complementary components to Npn transistors in many circuit designs. Pnp transistors utilize holes as the minority carrier in the diffusion-based transport across the n-type base. Because holes have lower mobility than electrons, Pnp transistors are slower and therefore generally less desirable than the Npn transistor. The primary motivation for development of the Pnp heterojunction bipolar transistor (HBT) discussed herein is not as a high speed component, but for government applications that require resistance to harsh environments, including mixed neutron and gamma irradiation. For circuits that require radiation resistance, devices specifically designed to maintain higher gain after radiation exposure should provide an advantage over parts not optimized for radiation performance. The heterojunction bipolar transistor (HBT) with the added design latitude afforded by bandgap engineering offers the potential for greater radiation hardness than the silicon bipolar junction transistor (BJT) (1).

An AlGaAs/GaAs Pnp HBT has been developed as an alternative to the commercially available Pnp BJT, but with improved radiation response (data not shown). However, the AlGaAs/GaAs material system poses several significant challenges in manufacturability which must be overcome to allow the Pnp HBT to be a viable alternative to the silicon Pnp BJT. It should be noted that the context of the manufacturability improvements are in a small fabrication facility with high involvement by experienced process personnel. The primary goal of this work was to minimize batch to batch variation and improve the robustness of a largely manual process.

Other material system options for the Pnp transistor include SiGe, InGaP/GaAs and InAlAs/InGaAs. SiGe capability is more established in a foundry setting; however the low volume and high voltage requirements did not provide incentive to support external

development. InGaP/GaAs and InAlAs/InGaAs were both investigated internally but will not be reported here.

In HBT device fabrication, wet etching reveals the emitter, base and collector layers of the structure and ohmic contacts are made on each surface to allow normal device operation. In addition, a ledge is created between the emitter and base to provide surface passivation, resulting in higher device gains. For optimal gain, thinning the base layer increases the probability of the minority carrier reaching the collector by minimizing the opportunity for recombination. The base layer should be thin enough to maintain adequate device performance yet thick enough for a reasonable base contact resistance and to allow enough etch margin to support high yield manufacturing.

A balance must be struck between the final base thickness and the ability to stop on and make contact to the base layer. Ammonium hydroxide / hydrogen peroxide and citric acid wet etches were investigated for their selectivity; however, neither provided an easily controlled etch necessary for our epitaxial structure. A wet etch stop grown at the top of the base layer was also not feasible without negatively impacting device performance. Therefore, extremely tight wet etch process control would be needed. To make contact to the n-type base, the anticipated post-anneal metal spiking of the traditional Ge/Au/Ni/Au n-type ohmic contact would be unacceptable. Non-spiking ohmic contacts were investigated to prevent shorting of the base to the underlying collector layer.

Improved wet etch control though the standard experimental strategies of reducing the etch rate and assessing the measurement accuracy and reproducibility of our metrology capabilities were evaluated; however, these alone were not sufficient to provide the needed depth control. The critical step was utilizing a PEVCD-deposited silicon nitride hard mask, not for etch selectivity, but for measurement accuracy. The hard mask provides a small step height and a smooth top surface for improved precision of the measurement - a significant improvement over the large step height and non-uniform surface morphology of a standard reflowed photoresist profile.

Experimental

AlGaAs/GaAs Pnp HBT epitaxial material was grown by molecular beam epitaxy at Sandia National Laboratories and processed in the Compound Semiconductor Research Laboratory (CSRL). The full HBT process has eleven photolithographic steps, four wet etch steps and four metallizations. The key experiments were around base metallization and emitter and ledge etch; all other process steps were held constant. The basic process with incorporated improvements is provided below and in cross-section in Figure 1.

The emitter metal stack of Ti/Pt/Au is deposited by e-beam evaporation onto an image reversed pattern for liftoff. A 1000Å plasma enhanced chemical vapor deposition (PECVD)-deposited silicon nitride hard mask protects the emitter metal during nonselective wet etching of InGaAs, GaAs and AlGaAs with 1:4:245 H_3PO_4 : H_2O_2 : H_2O to form the emitter mesa. Using the hard mask for the emitter etch is necessary to provide an accurate starting depth for the ledge etch. The ledge mesa wet etch is the most critical etch process, requiring termination in the very thin base layer. The silicon nitride hard mask and the 1:4:245 etch chemistry were also used for this etch.

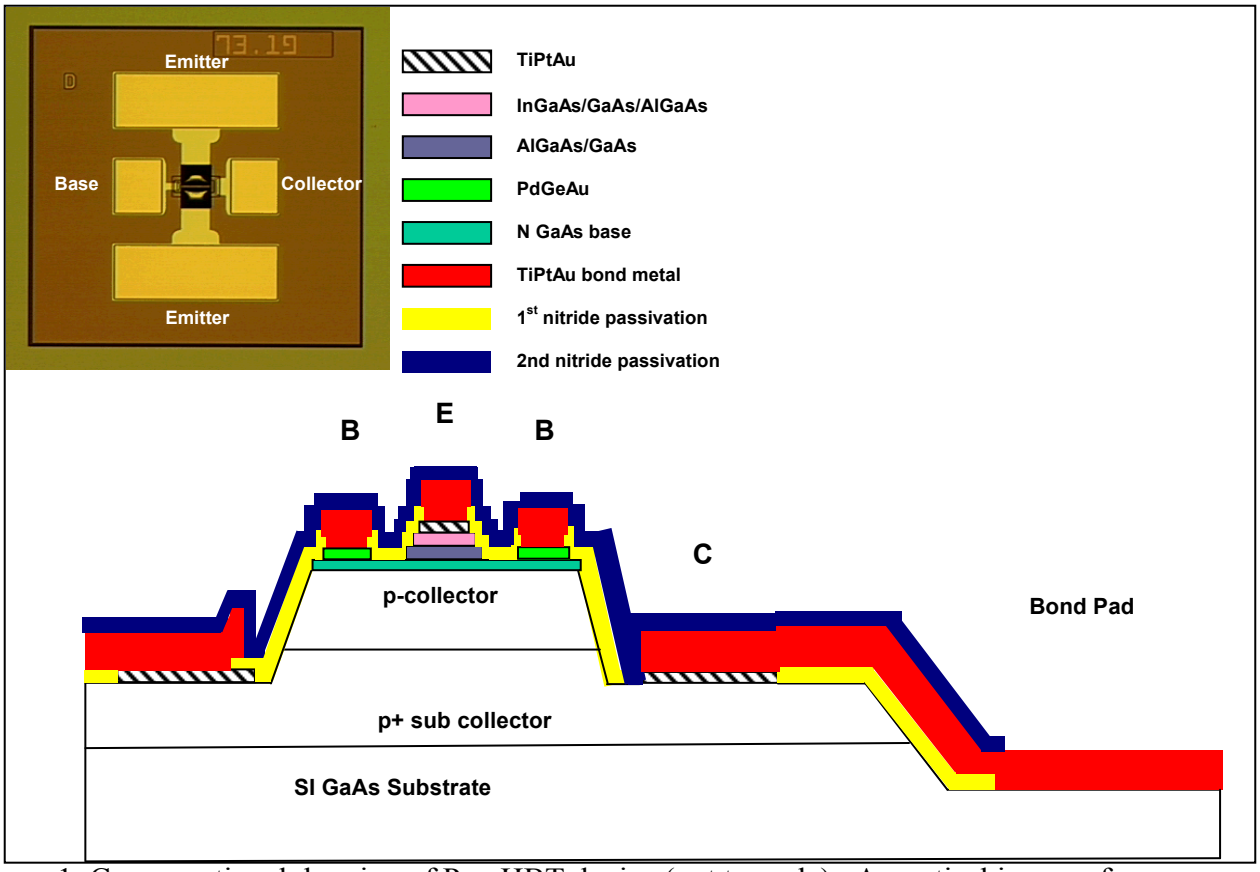

Figure 1. Cross-sectional drawing of Pnp HBT device (not to scale). An optical image of the AlGaAs/GaAs Pnp HBT is provided as an inset.

The base ohmic metallization was formed by e-beam evaporation and lift-off of Pd/Ge/Au, a non-spiking contact. The base mesa is wet etched in 1:4:45 H_3PO_4 : H_2O_2 : H_2O using a reflowed positive tone resist mask. Less stringent etch controls were required for this etch due to the relatively thick subcollector layer for the etch end point.

The collector ohmic metallization utilizes thermally evaporated BeAu on an image reversal resist pattern for liftoff. A rapid thermal anneal at 380°C for 30 seconds alloys the emitter, base and collector metals simultaneously. The device is isolated by etching the collector mesa to the semi-insulating GaAs substrate with 1:4:45 H_3PO_4 : H_2O_2 : H_2O. A reflowed positive tone resist mask was used.

A first layer of passivation of the entire structure is provided by PECVD silicon nitride. Vias are opened on the emitter, base, and collector contacts by reactive ion etching (RIE) using a positive tone resist mask. Nitride is also removed at the bond pad locations to allow the bond pads to contact the semi-insulating substrate. This improves metal adhesion, which is important for electrical testing and wire bond/packaging considerations. Cleave streets are also opened during this dry etch process.

A double-layer lift-off process is used to define the e-beam evaporated, thick Ti/Au bond pad metal. The entire structure receives a second PECVD silicon nitride passivation layer. The passivation film is opened by RIE to allow contact to the bond pads and to define streets necessary for singulation. Wafers are then lapped to 200µm and a thin Ti/Au backside metallization is deposited to facilitate packaging for the production devices.

Results and Discussion

A design of experiments (DOE) was performed to investigate several epitaxial structures and device designs aimed at improving the general manufacturability and understanding performance in relevant environments. Various epitaxial structures were grown and processed through the entire HBT process. The aspects of the DOE targeting manufacturability include base thickness, base doping and the addition of etch stops at the emitter and collector interfaces. Though the ledge etch is most critical, an etch stop to allow termination directly above this layer would adversely affect device performance, so was not included in this study.

The primary outputs monitored for the experiment were gain, base-collector breakdown voltage (BV_{CBO}) and leakage current (I_{CBO}), base-emitter breakdown voltage (BV_{EBO}) and leakage current (I_{EBO}), and radiation response (data not shown). Though not a completely isolated variable, the base thickness appears to follow the expected inverse square behavior for diffusive transport resulting in a gain decrease of roughly a factor of 3 for the thicker, 1000Å base when compared to the standard 600Å base. This was estimated by removing the calculated linear contribution of base doping, not considering interactions. Addition of the etch stops resulted in a significant increase in I_{CBO}, and was not considered further. The epitaxial design efforts to improve manufacturability did not result in a recommendation to change the baseline structure. Focus shifted to improving manufacturability of the HBT fabrication process.

Contacting the thin base layer was the first challenge to be overcome. The widely used Ge/Au/Ni/Au metal stack for ohmic contacts to n-type GaAs often results in superior contact resistance for many applications. However, AuGa can also form during anneal of the contact, resulting in metal spiking of a significant depth into the semiconductor (2). Ge/Au/Ni/Au contacts were investigated to determine the depth of spiking in our n-doped GaAs contact layer at the anneal temperature of 400°C. Cross-sectional SEM's showed spiking of up to 1000Å post-anneal, enough to penetrate the thin base layer and short to the collector. Therefore, contacts that exhibit little or no spiking into the semiconductor would be required.

Ti/Pt/Au, Pd/Ge/Pd, Pd/Ge/Ti/Au and Pd/Ge/Au were evaporated on bulk n-type $5 \times 10^{18} cm^{-3}$ GaAs to compare contact resistance from transmission line measurements (TLM's). These contacts are based on heavily doped surfaces or solid-phase regrowth which result in limited reactions with the GaAs surface, greatly decreasing the likelihood of spiking. (2) The Ti/Pt/Au contact was included in this study to observe the response for our doping level.

Pd/Ge/Au provided the lowest specific contact resistance by an order of magnitude as well as the best surface morphology. Cross-section SEM's shown in Figure 2 exhibited no observable spiking and electrical data for devices confirmed that the base was not shorted to the collector. Table I provides the results of the TLM's for each contact. Though the contact resistance values are not remarkably low, the results seen here were acceptable for our application. Further optimization of the metal constituent thicknesses and anneal conditions may improve the overall contact resistance. Ti/Pt/Au exhibited Schottky behavior due to the relatively low doping of the contact layer and is therefore omitted from the table.

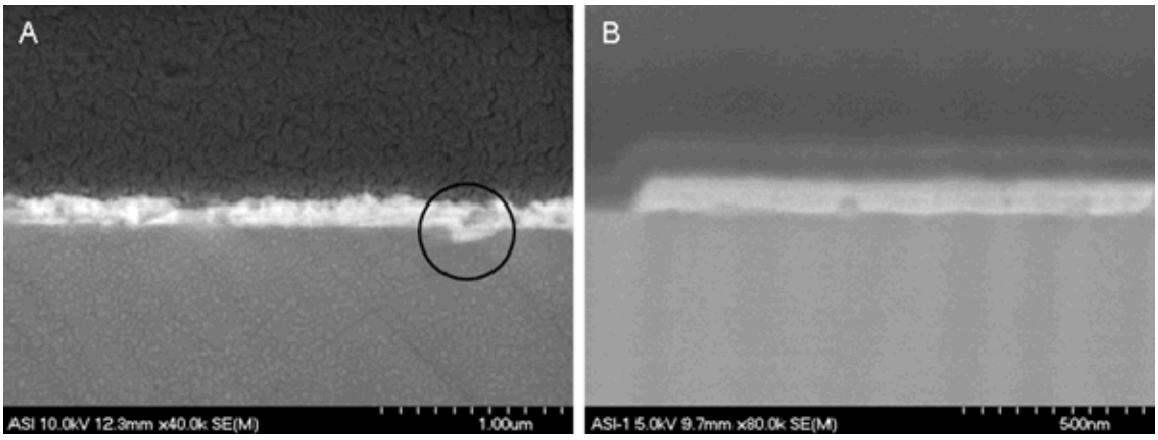

Figure 2. Cross-sectional SEM's for the Ge/Au/Ni/Au contact (A) and the Pd/Ge/Au contact (B). Note the spiking of the metal in the Ge/Au/Ni/Au sample.

TABLE I. Resistance comparison for non-spiking n-ohmic contacts.			
Contact	**R_sheet (Ω/□)**	**R_spec (Ω cm^2)**	**R^2**
Pd/Ge/Au	214.33	1.67E-06	0.99973
Pd/Ge/Ti/Au	215.97	1.10E-05	0.99115
Pd/Ge/Pd	215.67	1.24E-05	0.99996

The second challenge in improving manufacturability required tighter wet etch process control to accurately terminate the etch in the thin base layer. The standard etch chemistry used in our initial process utilized 1:4:45 H_3PO_4 : H_2O_2 : H_2O to nonselectively etch InGaAs, AlGaAs and GaAs. With an etch rate of nominally 50Å/s, the etch was difficult to stop in the 600Å base layer. By diluting the chemistry to a 1:4:245 ratio, the etch rate was reduced to 10Å/s, increasing the process window for etch time.

Accuracy of the etch rate and step height measurements were also of concern. Because etch stops are not grown in the epitaxial structure, an iterative wet etch process was necessary, dependent on accurate etch rates and frequent monitoring by profilometry measurements. Etch rate tests were implemented prior to the initiation of etching or whenever a new batch of chemical was used. The etch rate test was twice as long as a standard test used in 1:4:45 etching to reduce the noise of the etch depth measurement.

Studies were performed to compare two different profilometers and an atomic force microscope (AFM) to determine which measurement technique would be the best choice for our process. A standard product wafer was measured in designated locations on each tool multiple times (30 times per profilometer, 6 times on the AFM). It should be noted that fewer total measurements were taken on the AFM due to longer measurement time. As would be expected, the AFM provided the most reproducible measurement, especially when measuring the same location on the wafer; however the time required to set-up and complete the measurements was not conducive to our iterative wet etch process. As shown in Figure 3, Profilometer 2 had an overall range of 41Å, compared to a range of 60Å for Profilometer 1. The AFM was better than both of these at 23Å; however, with only an 18Å difference in the range, it was decided to use the least variable profilometer for ease of use and minimum set-up time.

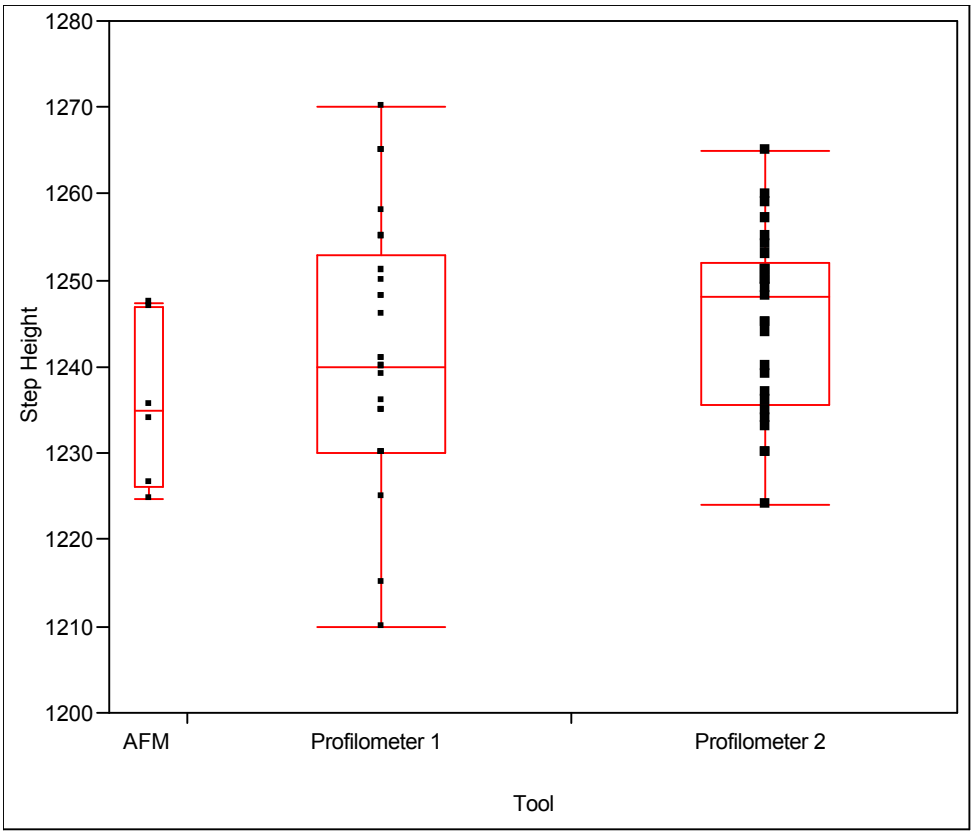

Figure 3. Step height versus tool to investigate tool variation. Note that the AFM has the least amount of variation (though the fewest measurements taken) and Profilometer 1 has the most variation.

With these basic improvements and controls in place, the largest source of error was the difficulty in reproducibly measuring the hard baked positive photoresist profile. Hard baking is needed to prevent resist attack during the wet etch; however the bake causes the resist to reflow, resulting in the resist being pulled toward the center of the feature, leaving an annular profile. The un-level surface caused measurement reproducibility to suffer. The added concerns of resist erosion or swelling during the wet etch could also be mitigated by developing a hard mask process.

A PECVD silicon nitride film was selected as a starting point for a hard mask. Silicon dioxide was not an option due to other considerations of our device. Pattern transfer was achieved by dry etching the nitride in a reactive ion etch tool using non-reflowed positive resist as a mask. The resist was then stripped in acetone to leave the patterned 1000Å thick PECVD nitride. Following the wet etch, the silicon nitride hard mask was removed in 6:1 buffered oxide etch (BOE). A wet process was selected for mask removal to avoid the potential for plasma damage with the exposed ledge. The nitride provided a very thin, smooth measurement surface. For comparison, a reflowed positive photoresist mask is several microns thick with an un-level surface, both of which impaired measurement repeatability. By changing to the hard mask, the measurement variation was reduced from a typical value of 500Å for the reflowed photoresist to less than 50Å.

After all of these changes were implemented into the HBT process, delamination of the emitter metal was observed on the small device geometries following removal of the nitride hard mask, thought to be associated with undercut of the titanium adhesion layer in the emitter metal stack (200Å Ti / 100Å Pt / 2000Å Au) during the hard mask removal

etch. A screening experiment was performed to test this theory. Three different Ti thicknesses (100Å, 200Å and 400Å) were deposited in the otherwise standard emitter metal scheme and etched at various hard mask removal etch times. TLM's on test wafers were concurrently run to monitor the effect of Ti thickness on contact resistance. Following emitter metal deposition, a variation of the hard mask removal etch was performed followed by a one minute high pressure acetone spray to induce lifting. Wafers were inspected to evaluate emitter metal delamination. Confocal microscopy was used to evaluate undercut for each of the samples. Figure 4 provides example images illustrating the observed undercut for the 200Å and 400Å Ti samples at 2 and 3 minutes of etching in 6:1 BOE. Note that the 100Å Ti samples and all samples etched for only 1 minute (which is not sufficient to completely remove the hard mask) do not show observable signs of undercut.

For each emitter metal stack variation (100Å, 200Å and 400Å Ti), test pieces from the same epitaxial wafer were processed as TLM's. The specific contact resistance values calculated from the TLM's were 8.85 x 10^{-6} Ωcm^2, 1.69 x 10^{-5} Ωcm^2 and 1.71 x 10^{5} Ωcm^2, respectively. With the primary benefit of improved adhesion due to less undercut, the specific contact resistance was also improved for the sample with 100Å Ti.

After observing the undercut on the experimental samples, a partially processed production wafer that had been scrapped for emitter metal delamination was examined with the confocal microscope and the same undercut signature was present. Optical profilometry was used to confirm that the area thought to be undercut in the micrograph exhibited a step height difference of approximately 200Å where the metal had sagged after the Ti had been removed by the BOE etch, shown in Figure 5.

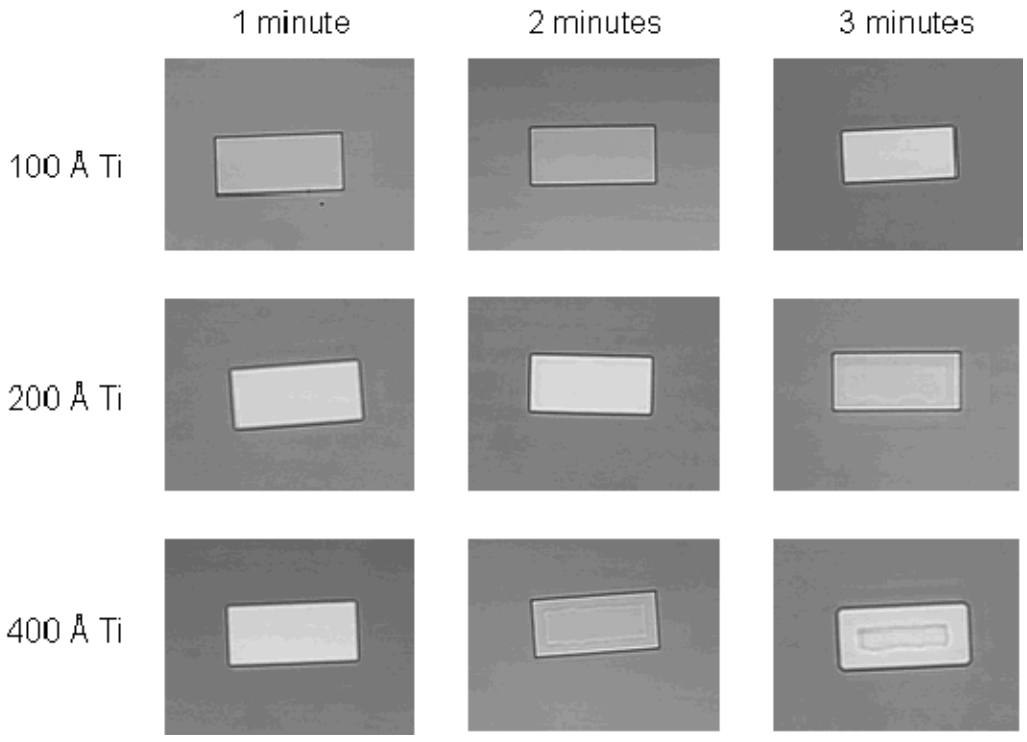

Figure 4. 100Å, 200Å and 400Å Ti in the emitter metal stack viewed by confocal microscopy for samples etched in 6:1 BOE for 1, 2 and 3 minutes. Note the apparent undercut for 200Å and 400Å Ti samples at times greater than 1 minute.

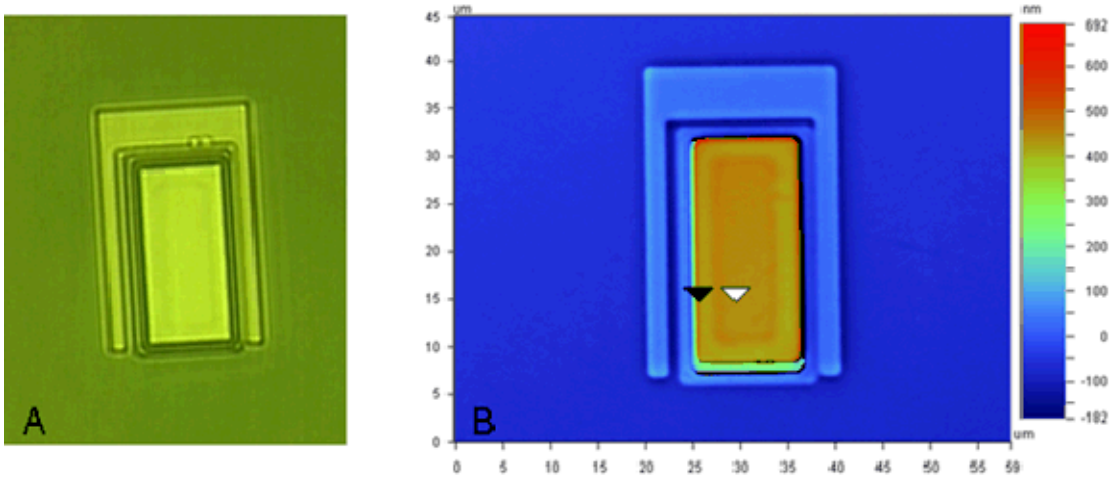

Figure 5. Confocal image of partially processed HBT showing Ti undercut on the emitter metal (A). Optical profilometry scan shows step height difference of the emitter metal (B) and confirms Ti undercut by showing ~250Å depression where the nominal 200Å Ti layer has been removed.

To further investigate the cause of the Ti undercut leading to emitter metal delamination and to determine specific process improvements that would eliminate the issue, a design of experiment (DOE) was utilized to explore possible failure modes. Dry etch removal of the hard mask was not pursued due to the anticipated effects of plasma damage on our devices following the wet etch to the base. Therefore, an alternate strategy had to be devised for removing the hard mask while maintaining emitter metal adhesion.

Potential identified failure modes resulting in emitter metal delamination included surface cleanliness, stress, Ti undercut and metal to semiconductor adhesion. Parameters varied to address these issues were pre-emitter metal deposition pre-cleans and oxygen descums, additional RTA's to encourage adhesion and potentially reduce stress following emitter metal liftoff, variation of the Ti thickness in the emitter metal stack and different strategies for nitride removal including not removing the hard mask at all. Experimental details of the DOE are provided in Table II with variations from the control in bold.

TABLE II. Emitter Metal Adhesion Experimental Details

Wafer	EM Descum	EM preclean	Ti Thickness	EM RTA	Nitride Removal
Control	5min 50W	10s 20:1 H_2O:NH_4OH	200Å	No	6:1 BOE
1	**4min 100W**	10s 20:1 H_2O:NH_4OH	200Å	No	6:1 BOE
2	5min 50W	**30s 10:1 H_2O/HCl**	200Å	No	6:1 BOE
3	5min 50W	10s 20:1 H_2O:NH_4OH	**100Å**	No	6:1 BOE
4	5min 50W	10s 20:1 H_2O:NH_4OH	200Å	**Yes**	6:1 BOE
5	5min 50W	10s 20:1 H_2O:NH_4OH	200Å	No	**HF**
6	5min 50W	10s 20:1 H_2O:NH_4OH	200Å	No	**Not removed**
7	**4min 100W**	10s 20:1 H_2O:NH_4OH	**100Å**	No	**HF**

Wafers were processed through the hard mask removal step (if applicable) following the wet etch into the base layer to expose the wafers to each of the steps likely to induce emitter metal delamination. Four hundred die from each wafer were 100% inspected by confocal microscopy to observe any preliminary metal lifting and to help quantify the outcome of each experiment. Results of this visual inspection quantification are provided

TABLE III. Emitter Metal Adhesion Experimental Results			
Wafer	**Variable**	**Change from Control**	**Yield**
Control	n/a	n/a	40%
1	EM Descum	4min 100W	63%
2	EM Preclean	30s 10:1 H_2O/HCl	62%
3	Ti Thickness	100Å	100%
4	EM RTA	Yes	100%
5	Nitride Removal	HF	43%
6	Nitride Removal	Not removed	100%
7	EM Descum Ti Thickness Nitride Removal	4min 100W 100 HF	100%

in Table III. Fully delaminated and devices with preliminary indication of lifting metal were counted as a yield loss.

Upon inspection, the only wafer that exhibited significant Ti undercut was the control. All other scenarios resulted in adhesion improvements. Ti undercut was confirmed to be the leading mechanism for the emitter metal delamination, as is evidenced by the drastic improvements with reduced Ti thickness and a change in the etch chemistry to HF. The thinner Ti would provide a smaller cross-section for Ti etching and undercut, resulting in a slower rate of etch. Switching from 6:1 BOE to HF is thought to result in less efficient wetting of the surface (due to the absence of surfactants in the HF), also resulting in less Ti undercut.

The data suggests that other causes may have also contributed. Surface preparation improvements shown in the emitter metal descum and preclean variations reduced emitter metal delamination alone by 37% and 38%, respectively, when compared to the yield of the control. Adding the RTA following emitter metal lift-off does encourage adhesion and resulted in no delamination in this experiment; however, the morphology of the contact became rough and was an undesired outcome of this additional step. Leaving the nitride hard mask on the device shows no delamination, as expected, due to the avoidance of the hard mask removal wet etch step that is the primary cause of the problem. However, leaving the mask in place had not been proven through the full HBT process. It was a concern that the presence of the nitride hard mask might induce stress or other unknown issues.

Wafer 7 was run to combine factors that were evaluated to have the lowest risk associated with implementation. This wafer also showed no delamination or preliminary evidence of lifting that could be visualized under confocal microscopy. Due to the low risk associated with each of the steps used for Wafer 7, all three were implemented in the final process flow. Representative optical micrographs are presented in Figure 6.

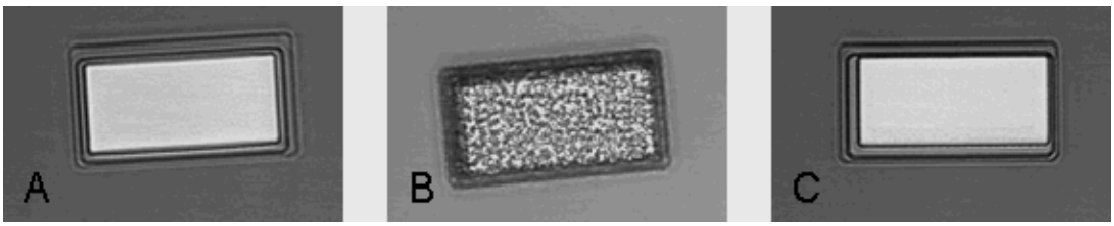

Figure 6. Representative confocal images for the second emitter metal adhesion experiments. Wafers 1-3 and 5-7 showed no undercut (A); wafer 4 exhibited surface morphology issues following RTA (B). Only the control exhibits observable Ti undercut (C).

The overall yield improvement is difficult to determine accurately. Wafers processed prior to the process improvement were likely 100% affected by Ti undercut in one of two ways. Some emitter metal exhibited Ti undercut as seen in Figures 4, 5 and 6. In other cases, the Ti was undercut to the extent that the emitter metal was completely missing from some devices. During subsequent processing steps, the bond pad metal applied to contact the emitter metal through a via in a passivating dielectric layer actually made acceptable contact to the emitter, resulting in functional devices. Though the gain was not significantly different than that of good devices, the long term reliability of the contacts smaller than the intended design (now defined by the size of the via) are likely to be less reliable. Additionally, the semiconductor-metal interface of this contact is likely to be less than ideal, due to potential contamination from the multiple processing steps that occur between the emitter metal delamination and the deposition of the bond pad metal. The devices that showed undercut (but not complete delamination) had a much lower gain than the delaminated devices, resulting in a bimodal distribution of gain. Resolving this issue produced a single gain distribution, as shown in Figure 7.

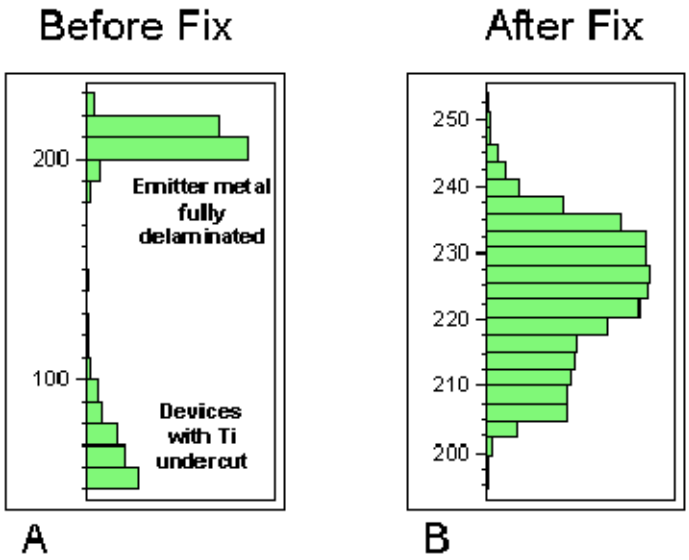

Figure 7. Device gain distributions measured at 10mA collector current. A bimodal distribution of gain can be seen prior to the hard mask removal process improvement (A). With the problem resolved, the gain displays a normal distribution (B).

Figure 8 illustrates the expected gain loss for devices with increased current density as a result of effective emitter area reduction by Ti undercut. Data shown is from devices of similar design at a comparable current density at 10mA collector current (I_c) to investigate the gain dependence on emitter area. Current density for a device of fixed emitter area increases with increasing I_c, so all current density and gain values referenced are at 10mA I_c for ease of comparison. A device with no Ti undercut has a current density of ~3200 A/cm^2. The gain for a similar device of the same current density is ~230. A device in which the Ti completely delaminates now has the emitter area defined by the via opening, resulting in a current density of ~3800A/cm^2. Data is shown for a similar device at 4000A/cm^2 with even higher gain. By reducing the emitter dimensions by 3 microns on each side (as shown by optical profilometry for the production device in Figure 5), the current density now more than doubles to ~8000 A/cm^2. Gain measured for a device of this current density is only ~50 because the gain has rolled over at a much

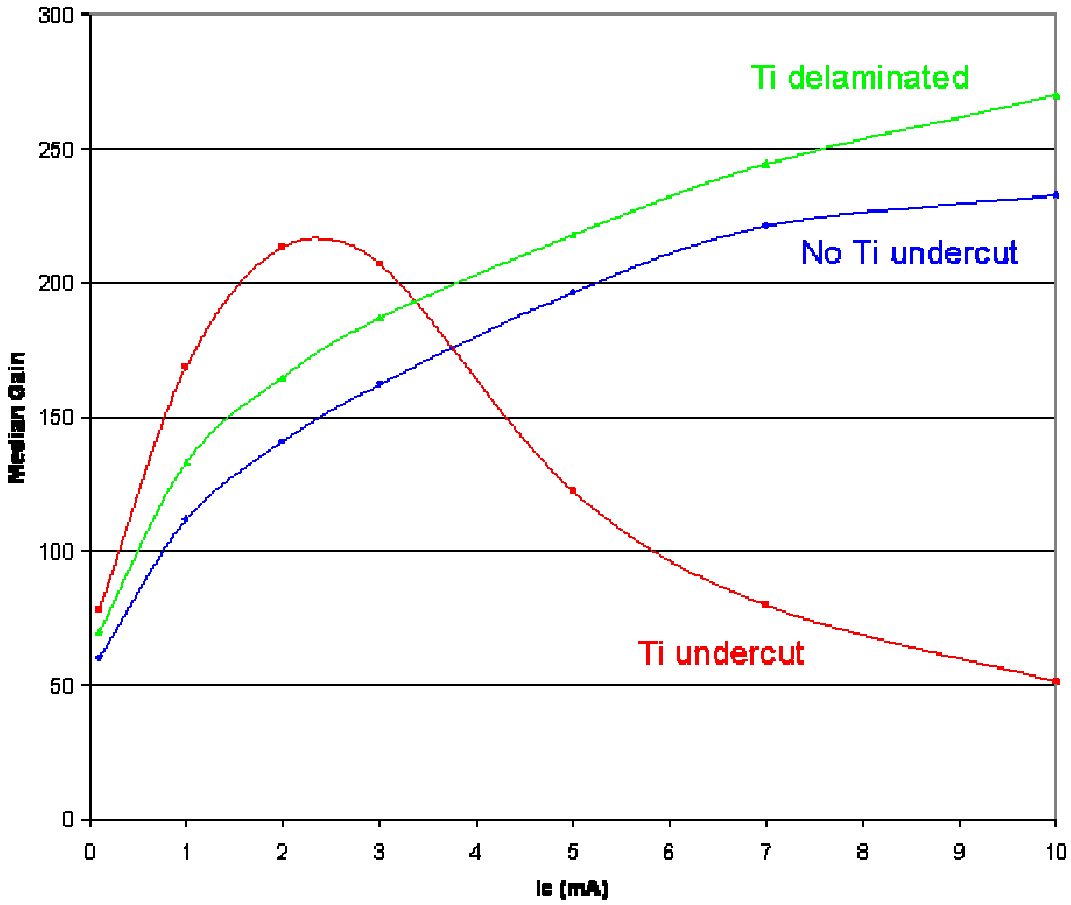

Figure 8. Device gain by collector current for devices with changes in current density that would be compatible for the change in the effective contact size for devices with and without Ti undercut.

lower I_c. These values generally agree with the gain loss that is seen in the bimodal distribution of those devices affected by the Ti undercut issue (Figure 7).

A possible explanation for the bimodal distribution is base push-out. Base push-out was observed in the electrical characteristics of all device designs investigated for the Pnp HBT's, typically at current densities of ≈ 6000 A/cm^2. This is due to the low mobility of holes in the reverse biased collector region near the base. At high current densities, the large hole density in the base region increases, effectively widening the base and decreasing the gain of the transistor. Another possible explanation may be that the emitter ohmic contact is not ohmic. A typical Gummel plot, shown in Figure 9, shows the base and collector currents as a function of base-emitter voltage with the base-collector terminals shorted together. Gummel plots for the initial device with Ti undercut and a device following implementation of the process improvements are shown. Series resistance is higher in the initial device, seen in the earlier deviation of the base and collector currents from linear on a semi-log plot. The devices with the final process show expected behavior in the Gummel plot.

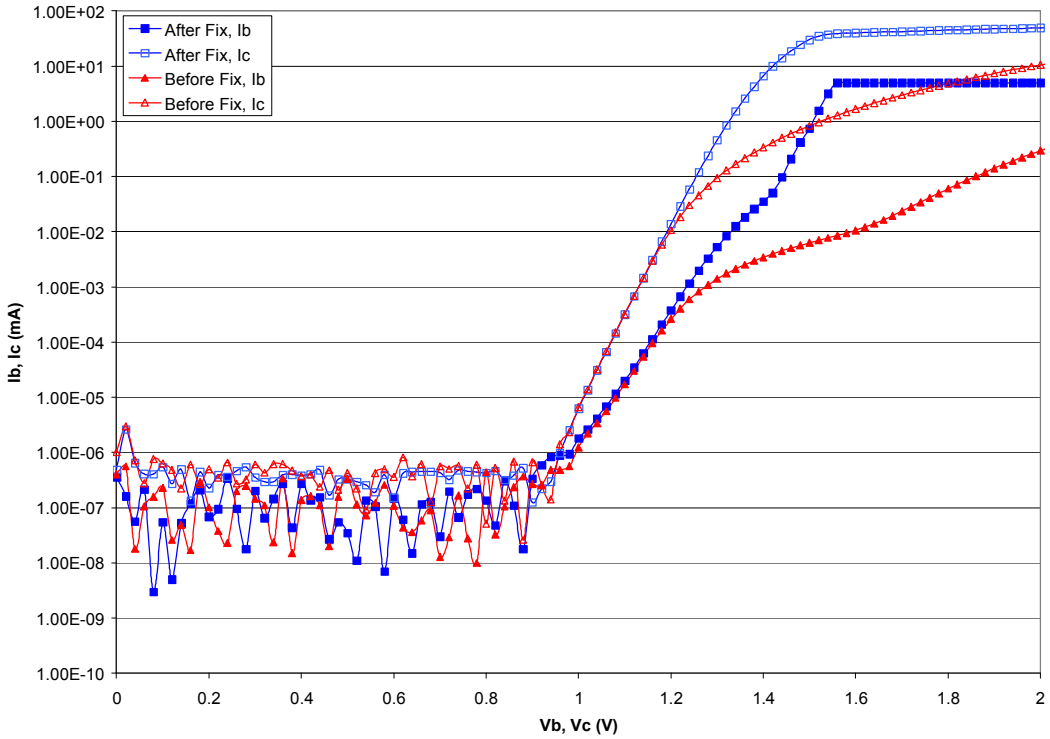

Figure 9. Gummel plot for devices after process improvement implementation (squares) and devices with Ti undercut (triangles). Note the higher series resistance in the devices with undercut contacts evidenced by the decreased base and collector currents at higher base and collector voltages.

Conclusions

Two key manufacturing challenges of the Pnp HBT in the AlGaAs/GaAs material system have been overcome. A wide array of relatively simple, low risk process improvements and process characterization efforts all contributed to a more reliable process. The implementation of these process improvements increased the average electrical yield from 43% to 90%. The significantly improved process control has made the radiation hard Pnp HBT a viable product replacement for the silicon BJT in various applications.

Acknowledgments

Sandia is a multiprogram laboratory operated by Sandia Corporation, a Lockheed Martin Company, for the United States Department of Energy's National Nuclear Security Administration under Contract DE-AC04-94AL85000.

References

1. J. B. Clevenger, G. A Patrizi, J. Klem, M. J. Cich, D. Chu, T. Peterson, S. Hawkins, D. King, S.M. Luker, V. Harper-Slaboszewicz, G. Hash, N. Kolb, L. Merriken, M. D. Martin,T. Fortune, A. G. Baca, P. J. Griffin, C. T. Sullivan , "Radiation Response of AlGaAs/GaAs Pnp Heterojunction Bipolar Transistors" to be presented at 2007 HEART Conference, March 5-9, San Diego, CA.

2. A. G. Baca, F. Ren, J. C. Zolper, R. D. Briggs, S. J. Pearton, *Thin Solid Films*, **309-309**, 559 (1997).